

# Nonrigid Matching of Undersampled Shapes via Medial Diffusion

Matthew Berger<sup>1,2</sup> and Claudio T. Silva<sup>3</sup>

<sup>1</sup>University of Utah

<sup>2</sup>Air Force Research Laboratory, Information Directorate

<sup>3</sup>Polytechnic Institute of New York University

---

## Abstract

We introduce medial diffusion for the matching of undersampled shapes undergoing a nonrigid deformation. We construct a diffusion process with respect to the medial axis of a shape, and use the quantity of heat diffusion as a measure which is both tolerant of missing data and approximately invariant to nonrigid deformations. A notable aspect of our approach is that we do not define the diffusion on the shape’s medial axis, or similar medial representation. Instead, we construct the diffusion process directly on the shape. This permits the diffusion process to better capture surface features, such as varying spherical and cylindrical parts, as well as combine with other surface-based diffusion processes. We show how to use medial diffusion to detect intrinsic symmetries, and for computing correspondences between pairs of shapes, wherein shapes contain substantial missing data.

Categories and Subject Descriptors (according to ACM CCS): I.3.3 [Computer Graphics]: Picture/Image Generation—Line and curve generation

---

## 1. Introduction

Matching of shapes undergoing nonrigid motion is an important problem in the area of geometry processing. The problem amounts to finding correspondences between shapes which adhere to the underlying deformation. It enables a wide number of applications such as registration, retrieval, object tracking, and shape interpolation.

For well-sampled shapes, finding correspondences under nonrigid motion has been well-studied, with effective solutions proposed by utilizing geodesics [TBW<sup>\*</sup>11], Möbius transformations [LF09], and the heat kernel [OMMG10]. For shapes which have been acquired via scanning, however, the resulting point cloud is often undersampled. Occlusion, material properties, and constrained resources such as a limited number of views can often result in the acquisition process producing incomplete data. For such point clouds it is necessary to construct quantities which are invariant to the motion and insensitive to the lack of data for successfully matching shapes.

In this paper we propose a method for constructing measures on undersampled shapes which are invariant to nonrigid motion. In particular, we use the medial axis as a prior to both model the deformation and infer the shape. Indeed,

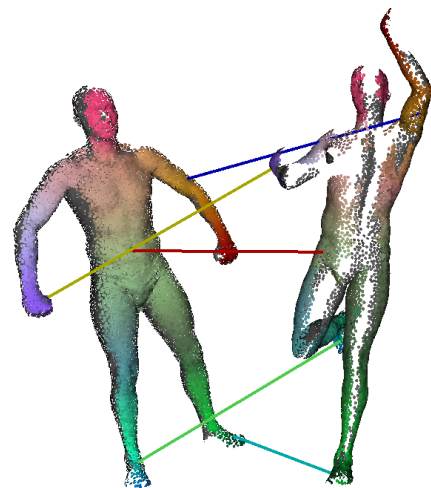


**Figure 1:** Our approach is able to match shapes undergoing nonrigid motion which contain significant missing data. Here we show the landmark correspondences automatically found by our algorithm, and the extrapolated dense mapping, color-mapped by the left shape’s medial embedding.

previous work has shown how the medial axis is invariant to pose [ZSM<sup>\*</sup>05], while also being robust to missing data in the construction of curve skeletons [TZCO09, LLZM10]. In fact the work of [ZST<sup>\*</sup>10] combined these two observations to match a collection of compact graph skeletons.

Our approach departs from [ZST<sup>\*</sup>10] and the usage of such compact representations by instead embracing the full point cloud, in conjunction with the medial axis prior, for shape matching. Inspired by heat kernel matching [OMMG10], we introduce *medial diffusion* for matching shapes, where matching amounts to finding points which belong to similar medial regions, see Figure 1. We seek correspondences between medial regions for such challenging point clouds, as there may exist a small amount of surface correspondences due to missing data, where in Figure 1 this is due to the shapes being scanned from opposing views.

Our main contribution is the construction of a Laplace operator defined with respect to the medial axis, for which its resulting heat kernel is suitable for shape matching. Key to our construction is that we define the operator *directly* on the point cloud. To define the Laplace operator we find that it suffices to measure the likelihood of pairs of points belonging to a mutually common medial ball, rather than utilizing an explicit geometric medial representation. This direct construction has a number of advantages:

- Our diffusion more faithfully represents the shape compared to curve skeleton methods, as these are inherently lossy representations, i.e. we can capture medial sheets.
- The diffusion process is sensitive to the geometry of the surface compared to skeletal representations, i.e. cylindrical regions of different radii exhibit distinct behavior.
- By working directly on the point cloud we can easily combine other diffusion processes.

From medial diffusion, we introduce a practical algorithm for finding landmark points between shapes, and subsequently extrapolating the landmarks to a dense correspondence of medial regions. Our approach also easily extends to detecting intrinsic symmetries, or nonrigid self-transformations. We show how our method is tolerant to missing data, and improves on standard heat kernel matching of incomplete shapes.

## 2. Related Work

Our approach is most closely related to three areas: medial representations, nonrigid registration, and finding correspondences.

**Medial Representations:** There exists a number of techniques for extracting medial representations from point clouds. For well-sampled point clouds, a specific subset of the Voronoi diagram, known as the Voronoi poles, has been shown to be a provably good approximation to the medial axis [ACK01]. For further processing, such a representation might be quite noisy, hence many methods exist

for simplified medial representations, such as the  $\lambda$ -medial axis [CL05] and the scaled axis transform [MGP10].

For dealing with incomplete point clouds the Voronoi poles become quite difficult to identify, and indeed may not exist. In these scenarios it is common to use a curve skeleton as the medial representation, as it has been shown to be a very useful shape prior. The method of [TZCO09] assumes a cylindrical prior for regions of missing data, so that only a small number of points in a cylindrical region need be used to find a medial structure. This was extended in [LLZM10] to better handle large gaps of missing data via a snake deformation model. These methods face robustness issues when the input fails to match the particular data prior.

**Nonrigid Registration:** Correspondence is a key component in the process of registering scans of a deforming shape, where missing data can frequently arise due to occlusion, limited views, and material properties. For time-varying capture, a number of approaches exist for computing correspondences, where they tend to rely on the coherence in motion between scan frames. Most of these approaches make assumptions either on templates, the acquisition process, or initialization. The approaches of [SWG08, LAGP09] rely on apriori defined templates to construct correspondences, since one can reliably construct geodesics on the template, which should remain invariant across the scanning sequence. The methods of [PSDB<sup>\*</sup>10, LLV<sup>\*</sup>12] rely on multiview stereo matching to initialize the dense matching of correspondences. Other approaches [WAO<sup>\*</sup>09, SAL<sup>\*</sup>08] rely on point-to-plane distance correspondences, which implicitly assumes that the motion between frames is small.

For a general collection of shapes, where frame-to-frame motion coherence is lost, correspondence becomes a much harder problem. The approach of [CZ08] relies on local features to extract a set of candidate correspondences. In the presence of missing data, however, it can be challenging to reliably construct local features. The methods of [LSP08, CZ09] instead rely on an initial overlap between point clouds, and consequently point-to-plane distance correspondences. A more sophisticated approach is the method of [HAWG08], where local features and geodesics are used to drive spectral matching. They use a k-nearest neighbor graph to construct geodesics, hence it is only reliable when the lack of data is consistent across scans.

**Finding Correspondences:** There are a large number of techniques for finding correspondences between well-sampled shapes, see [vKZHCO11] for an overview. The approach of [BBK06] applies generalized multidimensional scaling to find correspondences which best preserve geodesic distances. A deformation model is used in [ZSCO<sup>\*</sup>08] to measure the quality of correspondences, where quality is defined in terms of deformation distortion. Möbius voting [LF09] seeks to find correspondences which best preserve the conformal structure, thus allowing for a large space of deformations.

It is nontrivial to generalize the above approaches to point clouds, as they typically require a continuous surface representation, i.e. a triangulation. A notable exception is the method of [OMMG10], where they show how the heat kernel can be used to match nonrigid shapes, as the heat kernel is invariant to isometries. They demonstrate how their approach can be used for partial matching, as well as its insensitivity to small topological changes. Although used for meshes, the approach of [OMMG10] only requires a discretization of the Laplace-Beltrami operator, and numerous such discretizations exist for point clouds, see [BSW09, LSW09].

Little work has addressed the correspondence problem in the presence of large missing data. The work of [TBW<sup>\*</sup>09, TBW<sup>\*</sup>12] uses geodesic distances and a RANSAC-like approach to find landmark correspondences, which subsequently drives a dense correspondence matcher. They employ a k-nearest neighbor graph construction to approximate geodesics, hence they still require some coherence in the missing data for an accurate correspondence. Perhaps most similar to our work is [ZST<sup>\*</sup>10], where they employ the method of [TZCO09] to build a set of skeletons, and perform correspondence on the skeleton graphs. In some sense, we take an opposite approach while still using a medial axis prior, in that we consider the full point cloud rather than a compact skeletal graph.

### 3. Medial Diffusion

Our approach to constructing a diffusion process with respect to the medial axis of a shape is determined via a Laplace operator. We first discuss such a Laplace operator on a smooth surface, which we term the *Medial Laplacian*. We then detail its discretization on a point cloud, and lastly the diffusion process itself.

#### 3.1. Medial Laplacian

Consider an open set  $O$  embedded in  $\mathbb{R}^3$  whose boundary is the surface  $S$ . Every point  $\mathbf{x} \in O$  is associated with a set of points in  $S$  which are at a smallest distance to  $\mathbf{x}$ . We denote this set by  $\Gamma(\mathbf{x})$ . The set of points  $\mathbf{x} \in O$  for which  $|\Gamma(\mathbf{x})| \geq 2$  comprises the medial axis of  $O$ , which we denote by  $M$ .

The medial axis is a very descriptive object, as it carries the homotopy information of  $O$ . However, it is a rather difficult object to utilize, as it is composed of a set of adjoining sheets and curves. To define a Laplace operator directly on the medial axis, one option is to construct it piecewise for each sheet and curve, and handle special cases at junctions. One issue with proceeding in this way is that we lose information with respect to the geometry of  $S$ , for instance, spherical parts of varying radii are treated equally, as are cylindrical parts of different radii.

To better capture the surface, we use  $\Gamma$  as a density measure. As  $|\Gamma|$  is nonsmooth over  $M$ , denote  $|\tilde{\Gamma}|$  as its smoothed

variant, defined as:

$$|\tilde{\Gamma}(\mathbf{x})| = \int_S \exp\left(-\frac{d(\mathbf{z}, \Pi_{\mathbf{x}}(\mathbf{z}))}{\sigma}\right) d\mathbf{z} \quad (1)$$

Where  $\Pi_{\mathbf{x}}(\mathbf{z}) = \min_{\mathbf{y} \in \Gamma(\mathbf{x})} d(\mathbf{y}, \mathbf{z})$ , or the smallest geodesic distance  $d$  between the set  $\Gamma(\mathbf{x})$  and  $\mathbf{z}$ . We follow the approach of [BN08] to define a functional approximation to the Laplacian, in effect using a local Gaussian as an approximation. For a given function  $f$  defined on  $S$  we define the Medial Laplacian  $\Delta_M$  over  $M$  as:

$$\Delta_M f(\mathbf{p}) = f(\mathbf{p}) \int_M \alpha(\mathbf{p}, \mathbf{q}) |\tilde{\Gamma}(\mathbf{q})| d\mathbf{q} - \int_M f(\mathbf{q}) \alpha(\mathbf{p}, \mathbf{q}) |\tilde{\Gamma}(\mathbf{q})| d\mathbf{q} \quad (2)$$

Where  $\alpha(\mathbf{p}, \mathbf{q})$  is a Gaussian parameterized by a sufficiently small time scale  $h$ :  $\alpha(\mathbf{p}, \mathbf{q}) = e^{-\frac{|\mathbf{p}-\mathbf{q}|^2}{h}}$ .

We note that this is in fact a *weighted* Laplacian [BN08], where  $|\tilde{\Gamma}|$  is used to weight regions of the medial axis in which the number of closest points varies. Hence it is now sensitive to the surface area of  $S$ . Note that we can also approximate  $\Delta_M$  as an integral over  $S$  itself. If we denote for a given point  $\mathbf{x} \in S$  its corresponding point on the medial axis by  $\hat{\mathbf{x}}$ , then we define the Medial Laplacian  $\Delta_S$  over  $S$  as:

$$\Delta_S f(\mathbf{p}) = f(\hat{\mathbf{p}}) \int_S \alpha(\hat{\mathbf{p}}, \hat{\mathbf{q}}) d\mathbf{q} - \int_S f(\hat{\mathbf{q}}) \alpha(\hat{\mathbf{p}}, \hat{\mathbf{q}}) d\mathbf{q} \quad (3)$$

Note that the density measure  $|\tilde{\Gamma}|$  is implicitly included in the integration over  $S$ , since  $|\tilde{\Gamma}(\mathbf{x})|$  is the smoothed surface area over all points  $\Gamma(\mathbf{x})$ .

The Medial Laplacian is invariant to deformations on  $S$  which isometrically preserve its medial axis, while also preserving each point's ball radius. As demonstrated in previous work [ZSM<sup>\*</sup>05, ZST<sup>\*</sup>10], this property is often satisfied in real-world deformations, such as varying human pose. However, it is a smaller space of deformations than isometric deformations of  $S$  permit, whereas if we denote the Laplace-Beltrami operator of  $S$  by  $L_S$ , it is well-known that  $L_S$  is invariant to the space of all isometric deformations [SOG09]. Nonetheless, in the presence of missing data  $L_S$  can be very far from the Laplace-Beltrami operator of the true shape, where as we will show,  $\Delta_S$  remains tolerant to missing data.

#### 3.2. Point Cloud Medial Laplacian

We now illustrate our approach for discretizing the Medial Laplacian on a point cloud. Consider a point cloud  $P = \{\mathbf{p}_1, \mathbf{p}_2, \dots, \mathbf{p}_n\}$  accompanied with normals  $N = \{\mathbf{n}_1, \mathbf{n}_2, \dots, \mathbf{n}_n\}$ . Normals are either directly taken from the acquisition process, or if not available, then estimated via PCA and oriented with a minimum spanning tree approach.

One option for discretizing the Medial Laplacian is to consider its form defined directly on the medial axis –  $\Delta_M$ . However as previously discussed, there exists numerous approaches for estimating the medial axis, and in the presence of missing data each approach has various strengths

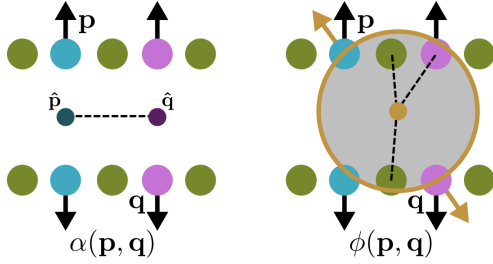


**Figure 2:** On the left we depict the distance between medial points  $\alpha$  to define the Medial Laplacian  $\Delta_S$ , while on the right we show medial similarity  $\phi$ , as an approximation to  $\alpha$ . Note that  $\phi$  does not require those points' corresponding medial axis points.

and drawbacks, hence it is unclear which to choose. Moreover, given a medial representation it is highly nontrivial to estimate each point's density  $|\tilde{\Gamma}|$ .

Hence we discretize  $\Delta_S$  instead, for two main reasons. First, we do not need to define  $\Gamma$ , as it is implicitly included in the integration. Secondly, we may interpret the distance between points on the medial axis,  $|\hat{p} - \hat{q}|$ , as the dissimilarity in medial regions between  $p$  and  $q$ . Hence it is not necessary to explicitly measure this distance, but rather construct the *likelihood* of two points belonging to a common medial ball, where we follow the approach of [BS12].

For every pair of points  $\mathbf{p}_i$  and  $\mathbf{p}_j$ , we construct a candidate ball of center  $\mathbf{c}_{ij}$  and radius  $r_{ij}$  which is representative of a potential medial ball on which  $\mathbf{p}_i$  and  $\mathbf{p}_j$  lie. We then measure how far away the candidate ball is from being a true medial ball. This is decomposed into two measures: how tangential is the candidate ball, denoted  $\tau$ , and how empty is the candidate ball, denoted  $\gamma$ :

$$\tau(\mathbf{p}_i, \mathbf{p}_j) = |\mathbf{n}_i - \mathbf{s}_i| + |\mathbf{n}_j - \mathbf{s}_j| \quad (4)$$

$$\gamma(\mathbf{p}_i, \mathbf{p}_j) = \sum_{\mathbf{p} \in P} \mu(\mathbf{c}_{ij}, r_{ij}, \mathbf{p}) \quad (5)$$

Here  $\mathbf{s}_i$  and  $\mathbf{s}_j$  are respectively the normals on the candidate ball at points  $\mathbf{p}_i$  and  $\mathbf{p}_j$ . The function  $\mu$  is a measure of how deep a given point  $\mathbf{p} \in P$  lies inside of the candidate ball, it increases as  $\mathbf{p}$  approaches  $\mathbf{c}_{ij}$ :

$$\mu(\mathbf{c}, r, \mathbf{p}) = \begin{cases} 1 - \left( \frac{|\mathbf{p} - \mathbf{c}|}{r} \right)^4 & \text{if } |\mathbf{p} - \mathbf{c}| < r \\ 0 & \text{otherwise} \end{cases} \quad (6)$$

We now arrive at our measure of medial similarity:

$$\phi(\mathbf{p}_i, \mathbf{p}_j) = e^{-\left(\frac{\gamma(\mathbf{p}_i, \mathbf{p}_j)}{\sigma_e}\right)^2 - \left(\frac{\tau(\mathbf{p}_i, \mathbf{p}_j)}{\sigma_t}\right)^2} \quad (7)$$

The measure  $\phi$  serves as an approximation to  $\alpha$ , see Figure 2 for an illustration. The parameters of  $\sigma_e$  and  $\sigma_t$  are analogous to the time scale  $h$ , where by increasing  $\sigma_e$  and  $\sigma_t$  we begin to associate points whose corresponding medial axis

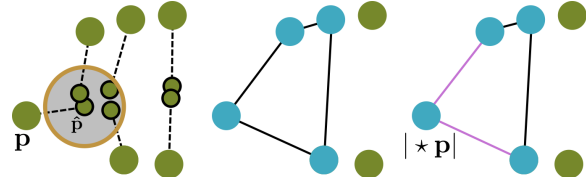


**Figure 3:** An illustration of dual area estimation for a point  $p$ : first we gather points which belong to a similar medial neighborhood, take these points' convex hull, and use the triangles incident to  $p$  to estimate its dual area.

points are further apart. We have found  $\sigma_e = 5$  and  $\sigma_t = 0.7$  to be suitable values, which we used for all results in the paper.

To discretize  $\Delta_S$  into the point cloud Medial Laplacian  $\Delta_P$ , we replace  $\alpha$  with  $\phi$  and follow the integral estimation approach of [BSW09]:

$$\Delta_P f(\mathbf{p}) = f(\mathbf{p}) \sum_{\mathbf{q} \in P} \phi(\mathbf{p}, \mathbf{q}) |\star \mathbf{q}| - \sum_{\mathbf{q} \in P} f(\mathbf{q}) \phi(\mathbf{p}, \mathbf{q}) |\star \mathbf{q}| \quad (8)$$

Where  $|\star \mathbf{q}|$  denotes the dual surface area which  $\mathbf{q}$  occupies.

**Area Estimation:** Crucial to an accurate discretization is an accurate estimation of the dual area at every point. The approach of [BSW09] defines the dual area at a point as the area formed by its local Delaunay triangulation. In the presence of missing data, this will effectively lead to the preservation of the inferred boundary components. We depart from [BSW09] and derive a more nonlocal method, based on our candidate ball centers. The basic idea is to find a neighborhood of points which belong to a similar medial region, and construct a triangulation from these points in the spirit of [BSW09], from which the dual area follows, see Figure 3 for an illustration of the method.

For each point  $\mathbf{p}_i \in P$  we estimate its corresponding medial axis point  $\hat{\mathbf{p}}_i$  and radius  $r_i$  by taking a weighted average of its candidate balls' centers and radii, respectively:

$$\hat{\mathbf{p}}_i = \frac{\sum_j \mathbf{c}_{ij} \phi(\mathbf{p}_i, \mathbf{p}_j)}{\sum_j \phi(\mathbf{p}_i, \mathbf{p}_j)} \quad r_i = \frac{\sum_j r_{ij} \phi(\mathbf{p}_i, \mathbf{p}_j)}{\sum_j \phi(\mathbf{p}_i, \mathbf{p}_j)} \quad (9)$$

We then gather all other points  $\mathbf{p}_j$  whose estimated medial axis points  $\hat{\mathbf{p}}_j$  are within a small  $\varepsilon$ :

$$B_i = \{\mathbf{p}_j \in P \mid |\hat{\mathbf{p}}_i - \hat{\mathbf{p}}_j| < \varepsilon\} \quad (10)$$

Where  $\varepsilon$  is fixed at 1.5 times the average sampling density of  $P$ . Intuitively,  $B_i$  consists of points who belong to a similar medial region of  $\mathbf{p}_i$ .

Next we take the convex hull of  $B_i$  and extract the set of triangles incident to  $\mathbf{p}_i$ . For concave regions  $\mathbf{p}_i$  may not reside on the convex hull, in such situations we project all of the points to the ball formed by  $(\hat{\mathbf{p}}_i, r_i)$ , and then take its convex hull's triangles incident to  $\mathbf{p}_i$ . The dual area  $|\star \mathbf{p}_i|$  follows as one-third of the area of all incident triangles.

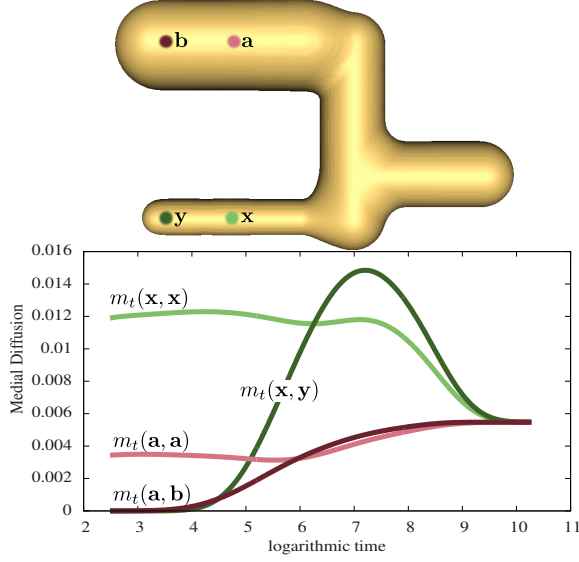


**Figure 4:** We illustrate the behavior of medial diffusion on the shape at the top, whose corresponding medial diffusion is plotted over time. Note that the diffusion is sensitive to the volume formed by the medial balls, where at **a** heat diffuses faster than **x**, hence it has a lower medial diffusion.

### 3.3. Medial Diffusion

We may now construct a diffusion process from the Medial Laplacian  $\Delta_S$ . The diffusion process is governed by the heat equation, which for a given function  $f$  defined over  $S$  is:

$$\Delta_S f(\mathbf{x}, t) = -\frac{\partial f(\mathbf{x}, t)}{\partial t} \quad (11)$$

We may then define the operator  $M_t = e^{-t\Delta_S}$ , where  $M_t f$  satisfies the heat equation for all  $t$ . Note that  $M_t f$  has the effect of diffusing  $f$  along the medial axis.

We can now associate a function  $m_t(\mathbf{x}, \mathbf{y})$  with  $M_t$  such that the following is satisfied:

$$M_t f(\mathbf{x}) = \int_S m_t(\mathbf{x}, \mathbf{y}) f(\mathbf{y}) d\mathbf{y} \quad (12)$$

Intuitively, for two points  $\mathbf{x}$  and  $\mathbf{y}$ ,  $m_t$  measures the amount of heat which has diffused between the two points in time  $t$ , where heat diffusion is restricted over the medial axis. We term this *medial diffusion*.

For a point cloud  $P$ , we approximate  $m_t$  through  $\Delta_P$ , using the fact that  $m_t$  can be computed from the eigenvectors ( $\Psi_i$ ) and eigenvalues ( $\lambda_i$ ) of  $\Delta_P$ :

$$m_t(\mathbf{x}, \mathbf{y}) = \sum_i e^{-\lambda_i t} \Psi_i(\mathbf{x}) \Psi_i(\mathbf{y}) \quad (13)$$

**Diffusion Properties:** Analogous to the heat kernel  $k_t$  associated with the Laplace-Beltrami operator [SOG09],  $m_t$  inherits the properties of its defining Laplacian  $\Delta_P$ . For example, given a point  $\mathbf{x}$ , if  $\mathbf{y} \in \Gamma(\hat{\mathbf{x}})$ , then  $m_t(\mathbf{x}, \mathbf{y})$  will be large

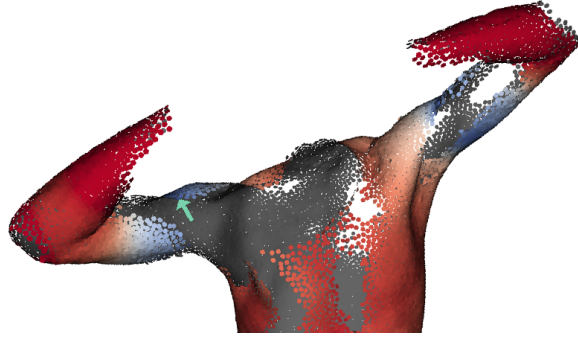


**Figure 5:** We illustrate medial diffusion as a shape signature, similar to [SOG09], where we depict the intrinsic symmetry of the shoulders. Note the lack of data on the lower-right shoulder, whereas the lower-left shoulder contains data yet is still recognized as having a similar signature.

for any time  $t$  – heat will immediately diffuse between the points. For regions containing varying ball radii, the medial diffusion will be sensitive to the surface area, see Figure 4 for an illustration. We see that for large cylindrical regions, the larger surface area results in fast heat dissipation, hence  $m_t$  will be low, whereas for smaller regions  $m_t$  will be larger.

More importantly, the diffusion is tolerant to missing data. Note that our association measure  $\phi$  captures nonlocal relationships. For regions of missing data where at least two points indicate a medial structure, heat will diffuse in a non-local manner. Combined with  $\Delta_P$ 's insensitivity to nonrigid deformations,  $m_t$  is a useful measure for identifying similar medial regions in incomplete shapes. In Figure 5 we illustrate  $m_t(\mathbf{x}, \mathbf{x})$  as a signature over a set of time scales  $t$ , similar to [SOG09]. Note that we are able to identify medial regions which are invariant to the pose.

**Insensitivity to Area:** Returning to our area estimation scheme, we find that dual areas can be somewhat noisy in regions which violate the medial axis prior. However, for our purposes, noisy areas are not too problematic, as we can claim the perturbation results of [SOG09]. Namely, we can write  $\Delta_P$  as  $\Delta_P = D^{-1}W$ , where  $W$  is the symmetric weight matrix and  $D$  is the diagonal matrix containing area weights. Now suppose that  $\tilde{\Delta}_P = (D+F)^{-1}(W+E)$ , where  $E$  and  $F$  are noise weight and area matrices, respectively, with  $\|E\| < \epsilon$  and  $\|F\| < \alpha$ . Denoting  $\tilde{M}_t$  as the heat operator of  $\tilde{\Delta}_P$ , then  $\|M_t - \tilde{M}_t\| = O(\sqrt{\alpha} + \epsilon)$ .

Intuitively, this means that the association measure between points, captured in  $W$ , has a larger impact on error than the area weights  $D$ . In our experiments, we have found that even if the estimated total surface areas between shapes are off by 10% – 15%, this has a negligible impact on our shape matching approach.

### 3.4. Combining Laplacians

An issue with medial diffusion is its behavior in regions of negative curvature, where the heat will diffuse very slowly, due to the large change in distance between medial axis points, as a function of small change in distance over the surface. This has an impact on nonrigid motion which results in significant volume change, i.e. regions containing negative curvature become zero or positive curvature. To address this, we can easily *combine* the standard Gaussian weight  $\alpha$  with the medial similarity weight  $\phi$ , so that the diffusion is less sensitive to negative curvature regions. Combining Laplace weights is common in spectral clustering, where in our situation, one may view the intrinsic geometry and the medial axis as multiple views of the same data [ZB07].

To combine Laplacians, we adapt the approach of [ZB07]. As  $\phi$  and  $\alpha$  have widely varying densities, they must be suitably normalized prior to being combined. To this end, consider the weighted summations for  $\phi$  and  $\alpha$ :

$$d_\phi(\mathbf{p}_i) = \sum_{j \neq i} |\star \mathbf{p}_j| \phi(\mathbf{p}_i, \mathbf{p}_j) \quad d_\alpha(\mathbf{p}_i) = \sum_{j \neq i} |\star \mathbf{p}_j| \alpha(\mathbf{p}_i, \mathbf{p}_j) \quad (14)$$

For a given interpolation factor  $\eta$ , we then combine the weights as [BN08]:

$$\sigma(\mathbf{p}_i, \mathbf{p}_j) = (1 - \eta) \frac{\phi(\mathbf{p}_i, \mathbf{p}_j)}{\sqrt{d_\phi(\mathbf{p}_i)d_\phi(\mathbf{p}_j)}} + \eta \frac{\alpha(\mathbf{p}_i, \mathbf{p}_j)}{\sqrt{d_\alpha(\mathbf{p}_i)d_\alpha(\mathbf{p}_j)}} \quad (15)$$

We then replace  $\phi$  in the definition of  $\Delta_P$  with  $\sigma$ .

We have used a value of  $\eta = 0.5$  for all results in the paper. Using this setting, we find that in most regions the medial similarity term  $\phi$  tends to dominate, and only in negative curvature regions  $\alpha$  has an impact in the diffusion.

## 4. Shape Matching

We now describe our approach in using  $m_t$  for matching shapes. We have adapted the approach of [OMMG10], which uses the observation that, given a single landmark correspondence,  $k_t$  can be used to infer all remaining correspondences. We apply this same methodology to  $m_t$  by finding a small set of landmark correspondences, and using them to extrapolate a dense matching of medial regions. We depart from [OMMG10] in how we find candidate correspondence points, and how  $P$  is sampled in order to evaluate the error of a potential matching. These modifications are necessary to handle point clouds containing missing data.

Given two point clouds to be matched,  $P$  and  $Q$ , we first uniformly subsample each with respect to the medial axis. We follow the approach of [BS12] by performing spectral clustering in the space of the diffusion maps formed by  $\Delta_P$  and  $\Delta_Q$ , where we denote the resulting subsets by  $S_P$  and  $S_Q$ . We found 700 points to be a sufficiently fine medial representation. This results in a set of points whose corresponding medial regions are uniformly spaced.

We then choose a point  $\mathbf{p}_l \in S_P$  at random, and for all points in  $S_Q$  we choose the  $\bar{\mathbf{q}}_l \in S_Q$  whose medial diffusion best matches  $\mathbf{p}_l$  over all points and time scales:

$$\bar{\mathbf{q}}_l = \operatorname{argmin}_{\mathbf{q}_l \in S_Q} \sum_{\mathbf{p} \in S_P} \min_{\mathbf{q} \in S_Q} |m_o^P(\mathbf{p}_l, \mathbf{p}) - m_o^Q(\mathbf{q}_l, \mathbf{q})| \quad (16)$$

Where  $m_o^P(\mathbf{p}, \mathbf{q})$  represents  $P$ 's medial diffusion over all times, similarly for  $Q$ . To realize this, we follow [SOG09] and logarithmically sample  $m$  over a discrete set of times, where we found 25 time scales to be sufficient, and each entry of  $m_t(\mathbf{p}, \mathbf{q})$  is divided by the heat trace at  $t$ . We may then embed  $m_o^P(\mathbf{p}, \mathbf{q})$  in a high dimensional space, and efficiently find  $\bar{\mathbf{q}}_l$ 's minimum  $\mathbf{q} \in S_Q$  through a kd-tree search, where we use the  $l_2$  norm. To avoid searching all of  $S_Q$  for the corresponding landmark, we only consider the top 5%  $\mathbf{q}_l \in S_Q$  whose signatures  $m_t(\mathbf{q}_l, \mathbf{q}_l)$  are closest to  $m_t(\mathbf{p}_l, \mathbf{p}_l)$ . The found  $\bar{\mathbf{q}}_l$  is unique up to the set of points which generate the medial axis point  $\bar{\mathbf{q}}_l$ . This redundancy is in part why our approach is robust – if the exact corresponding surface point is missing, we can instead assign a different point which generates the same medial axis point.

From this first landmark correspondence denoted  $(\mathbf{p}_l, \bar{\mathbf{q}}_l)$ , we greedily find additional correspondences via the same procedure, restricting the newly found correspondences to be consistent with the previous ones. This is accomplished by appending the previously found landmark coordinates to the new ones, as in [OMMG10]. We find new landmarks in  $S_P$  by performing a farthest-point sampling defined with respect to the diffusion map of  $\Delta_P$ . This has the effect of sampling landmark points in  $P$  which are far apart in the medial axis. We denote by  $L$  the set of landmark correspondences, where we found a total of 5 landmark correspondences to provide for sufficiently good results, corroborated by matching approaches [ZSCO\*08, KLF11] for well-sampled shapes.

We then use the  $|L|$  landmarks to extrapolate a dense set of correspondences between medial regions. This is accomplished by finding, for each  $\mathbf{p} \in P$ , the point  $\bar{\mathbf{q}} \in Q$  in which the medial diffusion is consistent across the respective landmarks, as well as the signature  $m_t(\mathbf{x}, \mathbf{x})$  [OMMG10]:

$$\bar{\mathbf{q}} = \operatorname{argmin}_{\mathbf{q} \in Q} \sum_{l=1}^L |m_o^P(\mathbf{p}_l, \mathbf{p}) - m_o^Q(\mathbf{q}_l, \mathbf{q})| + |m_o^P(\mathbf{p}, \mathbf{p}) - m_o^Q(\mathbf{q}, \mathbf{q})| \quad (17)$$

The initial randomly chosen landmark from  $S_P$  may be a rather non-descriptive feature with respect to  $S_Q$ , resulting in a poor matching. Hence we repeat this process (10 times in our experiments), and choose the matching which gives the lowest error in Equation 17, though a RANSAC-like approach [TBW\*09] could also be used.

## 5. Results

To evaluate our method, we have conducted two sets of experiments. First we measure the tolerance of our diffusion process to nonrigid motion and missing data. Secondly, we

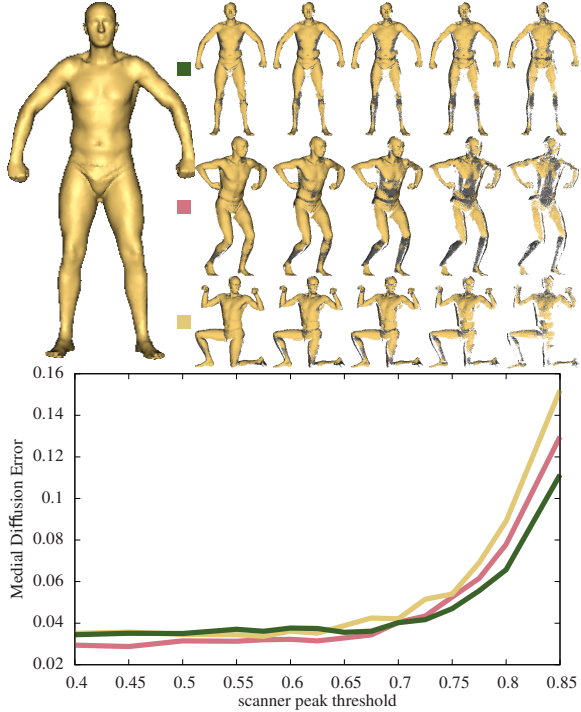


**Figure 6:** We measure the error in medial diffusion  $m_t$  across varying missing data and pose. We show the rest pose on the upper left, and on the upper right a subset of the poses and point clouds on which the rest pose is measured against.

have ran our matching algorithm across a set of shapes, and compared it with other similar shape matching methods.

We have used shapes in the SCAPE [ASP\*05], TOSCA [BBB\*08], and multi-view photometric stereo (MVPS) datasets [VPB\*09] in our experiments. For the TOSCA and SCAPE datasets we synthetically scan the shapes via the method of [BLN\*11], which models a laser-based optical triangulation scanner.

Regarding computational complexity, the largest amount of time spent in our method is constructing  $\Delta_P$ . For point clouds ranging in size from 15,000-20,000, it typically takes 5-9 minutes per shape to construct the Laplacian. Hence for all point clouds used we have subsampled them to within this range via farthest point sampling.

### 5.1. Tolerance to Missing Data

We first evaluate the quality of our method under varying pose and missing data. One way of achieving this is to extract the medial axis of a shape, and measure the geodesic distance distortion along the medial axis. However, the medial axis is well-known to be rather unstable, and the specific medial axis simplification approach to take (i.e. [CL05, MGP10]) is unclear.

Instead, we measure the error in  $m_t$ , in order to observe

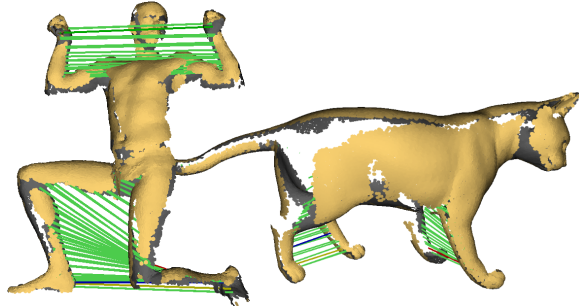


**Figure 7:** We show detected intrinsic symmetries between medial regions for point clouds containing missing data.

the consistency across pose and missing data. We use the SCAPE dataset, as ground truth correspondences are known. For a given SCAPE mesh, we synthetically scan it over a constant set of viewpoints via [BLN\*11]. We parameterize the peak threshold at which range is accepted based on the laser intensity, giving us a controllable yet realistic means of generating missing data. For a given well-sampled rest pose  $P$ , we measure the medial diffusion error on an input point cloud  $Q$  as:

$$E(P, Q) = \frac{1}{|C||T|} \sum_{t \in T} \left( \sum_{(\mathbf{x}, \mathbf{y}) \in C} |m_t(\mathbf{x}, \mathbf{y}) - m_t(f(\mathbf{x}), f(\mathbf{y}))|^2 \right)^{\frac{1}{2}} \quad (18)$$

Where  $C$  is a set of pairs of points uniformly sampled over  $Q$ ,  $T$  is the set of logarithmic time scales, and  $f$  is the ground truth mapping function between  $Q$  and  $P$ .

See Figure 6 for the results. As shown,  $m_t$  remains quite stable as missing data is introduced, over varying pose. Only when large gaps of data begin to appear does the error in  $m_t$  begin to increase. At these levels, the impact of the different poses becomes evident, as the rest pose contains the lowest error.

### 5.2. Intrinsic Symmetries

The detection of intrinsic symmetries follows as a straightforward extension of the shape matching method – rather than compare two shapes, we employ  $m_t$  on the same point cloud. Note that intrinsic symmetries in our situation refer to points along medial regions being invariant to a non-rigid self transformation. We visualize these correspondences by using the estimated medial ball centers  $\hat{\mathbf{p}}_t$ .

See Figure 7 for results on several shapes. Note that the front left leg of the cat point cloud is a separated component from the body, yet due to our method’s nonlocal diffusion we can still detect its symmetry with the front right leg.

### 5.3. Shape Matching

We now evaluate our matching approach across a set of shapes, compared with several approaches. To visualize the

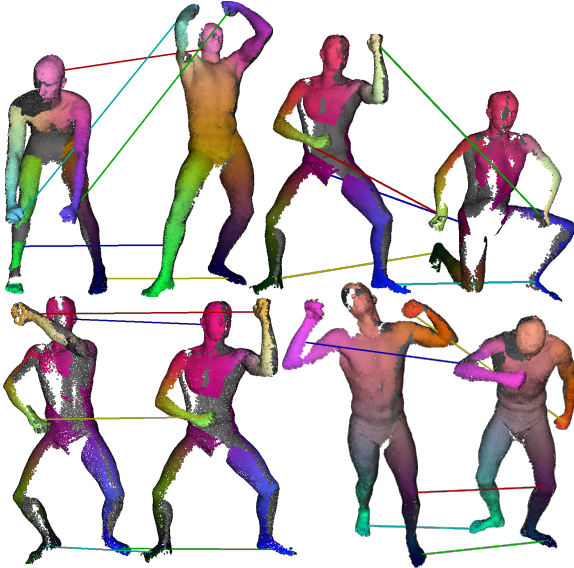


**Figure 8:** Correspondence results on the SCAPE dataset. On the top left pair, note the absence of data on the left shape’s stomach – we are able to infer that the back of the left shape and the stomach of the right shape share a medial region.

correspondences, for each point  $\mathbf{p}_i$  on the left shape we assign it a color based on the position of its estimated medial ball center  $\hat{\mathbf{p}}_i$ , and assign this same color to its corresponding point on the right shape.

Figure 8 shows our matching results on several shapes from the SCAPE dataset. As shown, our method is able to properly find landmark correspondences, and extrapolate a dense mapping between the shapes, despite the lack of data. In particular, note that the missing data is not consistent between the pairs of shapes, i.e. missing data occurs in different regions. Our method is shown to remain highly tolerant to these imperfections.

Figure 9 shows results for matching two different poses of the cat model from the TOSCA dataset. In the inset we depict the similarities of the medial diffusion signature  $m_t(\mathbf{x}, \mathbf{x})$  across the two point clouds. Note that the head of the left cat is a separated component from the rest of the body, yet we are still able to associate similarity to the neck of the right cat, despite the neck noticeably absent on the left cat.

In Figure 10 we compare our method with the skeleton extraction approach of [TZCO09] – the skeleton graphs used in [ZST<sup>\*</sup>10]. The compactness in the representation theoretically makes matching easier, yet as shown in the left shape, a node representing the head is absent, while an additional joint is introduced near the elbow, which makes matching rather ill-posed – it is unclear which to keep and which to prune. Our method incurs no such drawback by instead operating on the entire point cloud. Furthermore, note our

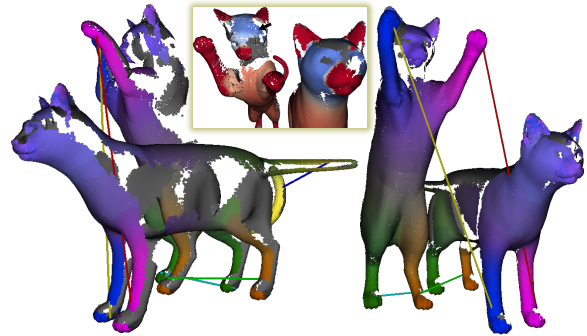


**Figure 9:** Correspondences for a pair of cat point clouds from the TOSCA dataset. In the inset, we depict the differences in the signature  $m_t(\mathbf{x}, \mathbf{x})$ , color-mapped across the two shapes. Note the signature’s insensitivity to the lack of data.

method’s ability to match medial sheets, shown across the chest, where by construction this is lost in [TZCO09].

Last, we have compared our method to the heat kernel matching approach of [OMMG10]. As [OMMG10] was originally designed for meshes, we instead use our strategy for finding candidate landmark points. We use the color-mapped positions  $\mathbf{p}_i$  to visualize their correspondences. See Figure 11 for the results. As shown, the heat kernel matching approach faces difficulty in finding landmark points for the SCAPE point clouds, hence the extrapolated correspondences are rather inaccurate. Our approach remains tolerant to the missing data. For the MVPS data, we see that [OMMG10] is able to properly find landmark correspondences for the “Abhijeet” sequence, yet the extrapolated correspondences are still imperfect. Our approach is able to properly match the right shoulder and head.

#### 5.4. Limitations

Although our method can handle a large range of incomplete shapes, it can perform poorly when the medial axis prior is not adequately satisfied. In particular, when the missing data is large relative to the size of the medial balls, then we may

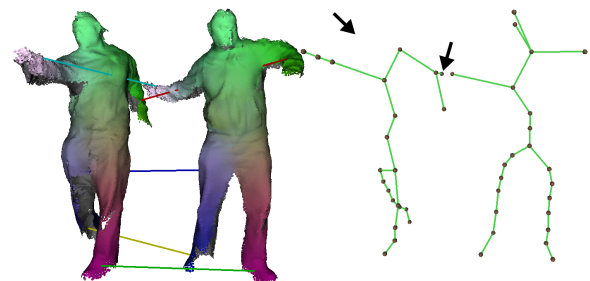


**Figure 10:** A comparison of our approach with skeletons extracted via [TZCO09]. Note the inconsistencies in the graph skeletons, which renders such matching rather ill-posed.

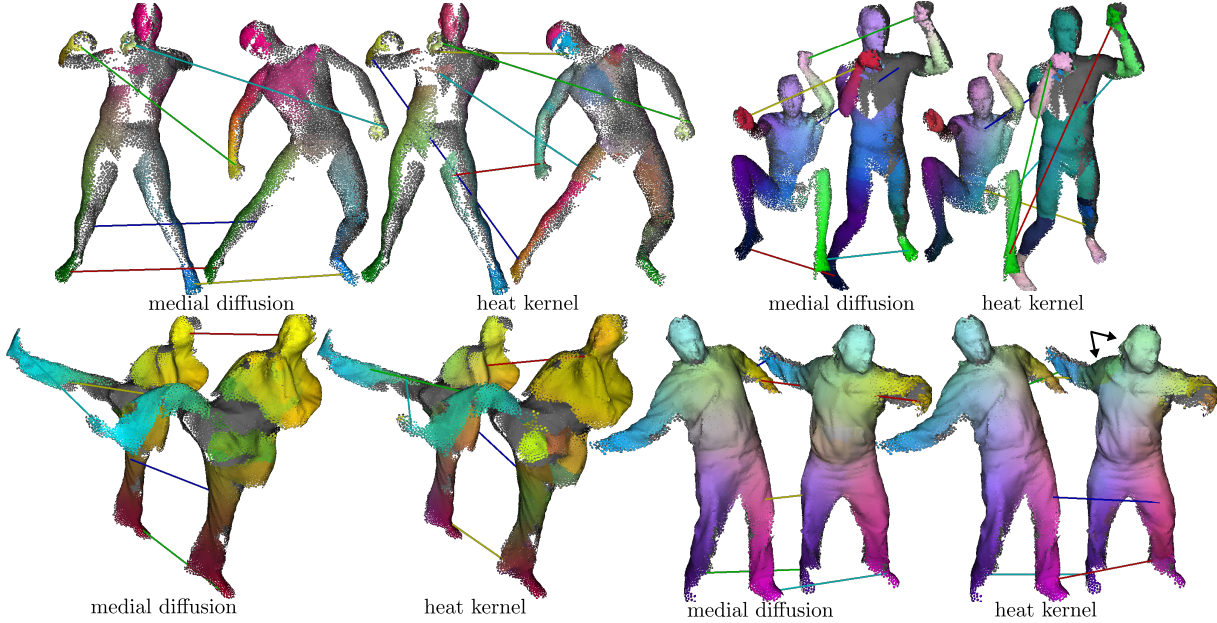


**Figure 11:** A comparison of our method with [OMMG10]. Note how we are able to find landmarks and good-quality extrapolated correspondences, whereas significant differences in the intrinsic structures of the shapes can pose problems for [OMMG10].

infer two separate connected components. In such situations it is difficult to construct a shape prior which this resembles, hence stronger priors such as templates may be necessary.

Like many other shape matching methods, our approach is vulnerable to symmetric flips [OHG11]. As the inset shows, our method can become confused by the inherent bilateral symmetry. However, it should be possible to use either a deformation-driven approach [ZSCO\*08], or combining a collection of matches [KLF11], in order to resolve this limitation.



Our method is fairly robust to deformations resulting in small changes to volume, but significant volume change can be problematic. For instance, substantial folding of cloth or fluid motion can result in drastic, non-isometric changes to the medial axis. Constructing a measure which is tolerant to such deformations, as well as incomplete data, is a challenging and important area for future work.

## 6. Conclusions

We have presented a method for matching incomplete shapes undergoing nonrigid motion. Our main contribution is the construction of a diffusion process on the point cloud which measures heat diffusion along the medial axis. As the medial axis is a strong prior for missing data, we have shown how

heat diffuses in a nonlocal manner, insensitive to both nonrigid motion and missing data, and how this may be used for matching incomplete shapes.

For future work, we would like to explore applications of our correspondences. In particular, correspondences between medial regions should benefit volume-based applications such as co-segmentation, style transfer, and shape retrieval. We also intend to investigate the theoretical properties of our construction of the Medial Laplacian. For instance, we would like to obtain a more explicit relationship between our medial dissimilarity measure and the distance between points on the medial axis.

## Acknowledgements

We thank Andrea Tagliasacchi for the skeleton extraction code and Lucas Sabalka for the useful feedback. This work was partially funded by the National Science Foundation and the Department of Energy Office of Science.

## References

- [ACK01] AMENTA N., CHOI S., KOLLURI R.: The power crust. In *Proceedings of the sixth ACM symposium on Solid modeling and applications* (2001), ACM, pp. 249–266. 2
- [ASP\*05] ANGUELOV D., SRINIVASAN P., PANG H., KOLLER D., THRUN S., DAVIS J.: The correlated correspondence algorithm for unsupervised registration of nonrigid surfaces. *Advances in neural information processing systems 17* (2005), 33–40. 6

- [BBBK08] BRONSTEIN A., BRONSTEIN M., BRONSTEIN M., KIMMEL R.: *Numerical geometry of non-rigid shapes*. Springer-Verlag New York Inc, 2008. 6
- [BBK06] BRONSTEIN A., BRONSTEIN M., KIMMEL R.: Generalized multidimensional scaling: a framework for isometry-invariant partial surface matching. *Proceedings of the National Academy of Sciences of the United States of America* 103, 5 (2006), 1168–1172. 2
- [BLN<sup>\*</sup>11] BERGER M., LEVINE J., NONATO L., TAUBIN G., SILVA C.: *An End-to-End Framework for Evaluating Surface Reconstruction*. SCI Technical Report UUSCI-2011-001, SCI Institute, University of Utah, 2011. 6, 7
- [BN08] BELKIN M., NIYOGI P.: Towards a theoretical foundation for laplacian-based manifold methods. *Journal of Computer and System Sciences* 74, 8 (2008), 1289–1308. 3, 6
- [BS12] BERGER M., SILVA C.: Medial kernels. *Computer Graphics Forum* 31, 2 (2012), 795–804. 4, 6
- [BSW09] BELKIN M., SUN J., WANG Y.: Constructing laplace operator from point clouds in r d. In *Proceedings of the twentieth Annual ACM-SIAM Symposium on Discrete Algorithms* (2009), pp. 1031–1040. 3, 4
- [CL05] CHAZAL F., LIEUTIER A.: The  $\lambda$ -medial axis. *Graphical Models* 67, 4 (2005), 304–331. 2, 7
- [CZ08] CHANG W., ZWICKER M.: Automatic registration for articulated shapes. In *Computer Graphics Forum* (2008), vol. 27, pp. 1459–1468. 2
- [CZ09] CHANG W., ZWICKER M.: Range scan registration using reduced deformable models. In *Computer Graphics Forum* (2009), vol. 28, pp. 447–456. 2
- [HAWG08] HUANG Q., ADAMS B., WICKE M., GUIBAS L.: Non-rigid registration under isometric deformations. In *Computer Graphics Forum* (2008), vol. 27, pp. 1449–1457. 2
- [KLF11] KIM V., LIPMAN Y., FUNKHOUSER T.: Blended intrinsic maps. *ACM Transactions on Graphics (TOG)* 30, 4 (2011), 79. 6, 9
- [LAGP09] LI H., ADAMS B., GUIBAS L., PAULY M.: Robust single-view geometry and motion reconstruction. *ACM Transactions on Graphics (TOG)* 28, 5 (2009), 175. 2
- [LF09] LIPMAN Y., FUNKHOUSER T. A.: Möbius voting for surface correspondence. *ACM Trans. Graph.* 28, 3 (2009). 1, 2
- [LLV<sup>\*</sup>12] LI H., LUO L., VLASIC D., PEERS P., POPOVIĆ J., PAULY M., RUSINKIEWICZ S.: Temporally coherent completion of dynamic shapes. *ACM Transactions on Graphics (TOG)* 31, 1 (2012), 2. 2
- [LLZM10] LI G., LIU L., ZHENG H., MITRA N. J.: Analysis, reconstruction and manipulation using arterial snakes. *ACM Trans. Graph.* 29 (December 2010), 152:1–152:10. 2
- [LSP08] LI H., SUMNER R., PAULY M.: Global correspondence optimization for non-rigid registration of depth scans. In *Computer Graphics Forum* (2008), vol. 27, pp. 1421–1430. 2
- [LSW09] LUO C., SUN J., WANG Y.: Integral estimation from point cloud in d-dimensional space: A geometric view. In *Proceedings of the 25th annual symposium on Computational geometry* (2009), ACM, pp. 116–124. 3
- [MGP10] MIKLOS B., GIESEN J., PAULY M.: Discrete scale axis representations for 3d geometry. *ACM Transactions on Graphics (TOG)* 29, 4 (2010), 101. 2, 7
- [OHG11] OVSJANIKOV M., HUANG Q., GUIBAS L.: A condition number for non-rigid shape matching. In *Computer Graphics Forum* (2011), vol. 30, pp. 1503–1512. 8
- [OMMG10] OVSJANIKOV M., MÉRIGOT Q., MÉMOLI F., GUIBAS L. J.: One point isometric matching with the heat kernel. *Computer Graphics Forum* 29, 5 (2010), 1555–1564. 1, 2, 3, 6, 8, 9
- [PSDB<sup>\*</sup>10] POPA T., SOUTH-DICKINSON I., BRADLEY D., SHEFFER A., HEIDRICH W.: Globally consistent space-time reconstruction. In *Computer Graphics Forum* (2010), vol. 29, pp. 1633–1642. 2
- [SAL<sup>\*</sup>08] SHARF A., ALCANTARA D., LEWINER T., GREIF C., SHEFFER A., AMENTA N., COHEN-OR D.: Space-time surface reconstruction using incompressible flow. In *ACM Transactions on Graphics (TOG)* (2008), vol. 27, ACM, p. 110. 2
- [SOG09] SUN J., OVSJANIKOV M., GUIBAS L.: A concise and provably informative multi-scale signature based on heat diffusion. In *Computer Graphics Forum* (2009), vol. 28, pp. 1383–1392. 3, 5, 6
- [SWG08] SÜSSMUTH J., WINTER M., GREINER G.: Reconstructing animated meshes from time-varying point clouds. In *Computer Graphics Forum* (2008), vol. 27, pp. 1469–1476. 2
- [TBW<sup>\*</sup>09] TEVS A., BOKELOH M., WAND M., SCHILLING A., SEIDEL H.: Isometric registration of ambiguous and partial data. In *Computer Vision and Pattern Recognition, 2009. CVPR 2009. IEEE Conference on* (2009), Ieee, pp. 1185–1192. 3, 6
- [TBW<sup>\*</sup>11] TEVS A., BERNER A., WAND M., IHRKE I., SEIDEL H.-P.: Intrinsic shape matching by planned landmark sampling. *Computer Graphics Forum* 30, 2 (2011), 543–552. 1
- [TBW<sup>\*</sup>12] TEVS A., BERNER A., WAND M., IHRKE I., BOKELOH M., KERBER J., SEIDEL H.: Animation cartography - intrinsic reconstruction of shape and motion. *ACM Transactions on Graphics (to appear)* 31, 2 (2012). 3
- [TZCO09] TAGLIASACCHI A., ZHANG H., COHEN-OR D.: Curve skeleton extraction from incomplete point cloud. *ACM Trans. Graph.* 28 (July 2009), 71:1–71:9. 2, 3, 8
- [vKZHCO11] VAN KAICK O., ZHANG H., HAMARNEH G., COHEN-OR D.: A survey on shape correspondence. *Computer Graphics Forum* 30, 6 (2011). 2
- [VPB<sup>\*</sup>09] VLASIC D., PEERS P., BARAN I., DEBEVEC P., POPOVIĆ J., RUSINKIEWICZ S., MATUSIK W.: Dynamic shape capture using multi-view photometric stereo. In *ACM Transactions on Graphics (TOG)* (2009), vol. 28, ACM, p. 174. 6
- [WAO<sup>\*</sup>09] WAND M., ADAMS B., OVSJANIKOV M., BERNER A., BOKELOH M., JENKE P., GUIBAS L., SEIDEL H., SCHILLING A.: Efficient reconstruction of nonrigid shape and motion from real-time 3d scanner data. *ACM Transactions on Graphics (TOG)* 28, 2 (2009), 15. 2
- [ZB07] ZHOU D., BURGES C.: Spectral clustering and transductive learning with multiple views. In *Proceedings of the 24th international conference on Machine learning* (2007), ACM, pp. 1159–1166. 6
- [ZSCO<sup>\*</sup>08] ZHANG H., SHEFFER A., COHEN-OR D., ZHOU Q., VAN KAICK O., TAGLIASACCHI A.: Deformation-driven shape correspondence. In *Computer Graphics Forum* (2008), vol. 27, pp. 1431–1439. 2, 6, 9
- [ZSM<sup>\*</sup>05] ZHANG J., SIDDIQI K., MACRINI D., SHOKOUFANDEH A., DICKINSON S.: Retrieving articulated 3-d models using medial surfaces and their graph spectra. In *Energy minimization methods in computer vision and pattern recognition* (2005), Springer, pp. 285–300. 2, 3
- [ZST<sup>\*</sup>10] ZHENG Q., SHARF A., TAGLIASACCHI A., CHEN B., ZHANG H., SHEFFER A., COHEN-OR D.: Consensus skeleton for non-rigid space-time registration. *Computer Graphics Forum* 29, 2 (2010), 635–644. 2, 3, 8